Automatica 83 (2017) 206–219

Contents lists available at ScienceDirect

Automatica

journal homepage: www.elsevier.com/locate/automatica

State-of-Charge estimation from a thermal–electrochemical model of lithium-ion batteries☆

Shu-Xia Tang [a], Leobardo Camacho-Solorio [a], Yebin Wang [b], Miroslav Krstic [a]

[a] Department of Mechanical & Aerospace Engineering, University of California, San Diego, La Jolla, CA 92093-0411, USA
[b] Mitsubishi Electric Research Laboratories, 201 Broadway, Cambridge, MA 02139, USA

ARTICLE INFO

Article history:
Received 4 August 2016
Received in revised form 10 February 2017
Accepted 19 May 2017

Keywords:
Infinite dimensional systems
Lithium-ion batteries
Battery management systems
PDE backstepping

ABSTRACT

A thermal–electrochemical model of lithium-ion batteries is presented and a Luenberger observer is derived for State-of-Charge (SoC) estimation by recovering the lithium concentration in the electrodes. This first-principles based model is a coupled system of partial and ordinary differential equations, which is a reduced version of the Doyle–Fuller–Newman model. More precisely, the subsystem of Partial Differential Equations (PDEs) is the Single Particle Model (SPM) while the Ordinary Differential Equation (ODE) is a model for the average temperature in the battery. The observer is designed following the PDE backstepping method. Since some coefficients in the coupled ODE–PDE system are time-varying, this results in the time dependency of some coefficients in the kernel function system of the backstepping transformation and it is non-trivial to show well-posedness of the latter system. Adding thermal dynamics to the SPM serves a two-fold purpose: improving the accuracy of SoC estimation and keeping track of the average temperature which is a critical variable for safety management in lithium-ion batteries. Effectiveness of the estimation scheme is validated via numerical simulations.

1. Introduction

1.1. Motivation

Due to its high power and energy storage density, its lack of memory effect and low self discharge, lithium-ion technology is a common choice among the rechargeable battery family (Chu & Majumdar, 2012). Besides its wide employment in portable electronics, lithium-ion batteries are now being adopted in electrified transportation (Stewart, Christensen, Chaturvedi, & Kojic, 2015) such as electric vehicles and hybrid electric vehicles. Lithium-ion technology is being considered for grid energy storage as well.

The key indicator for the amount of electrical energy available in batteries is the SoC which, simply put, is the ratio of instantaneous remaining battery charge to its maximum capacity (Chaturvedi, Klein, Christensen, Ahmed, & Kojic, 2010). Thus, in order to predict the available power and energy in the battery during operation, online estimation of the SoC serves as an important factor for regulating both charging and discharging. Besides, it is generally required that the SoC remains within appropriate bounds all the time during the battery operation for safety reasons. Hence, a reliable and accurate estimation of the SoC is required for proper battery management.

1.2. Lithium-ion battery models

Accuracy of the SoC estimation depends highly on the quality of the selected model. Thus, one is encouraged to compare the different models available for describing the battery dynamics. Models for lithium-ion batteries can be categorized into two classes. The first class consists of empirical models, in which the most frequently used ones are Equivalent Circuit Models (ECMs) (Chiasson & Vairamohan, 2005; Plett, 2004). ECMs use electric circuit elements such as voltage sources, resistances and RC networks to approximate the dynamics of the battery. Currently, most battery management systems employ ECMs for various tasks: power and energy estimation, cell balancing, thermal management, state-of-health estimation and charge/discharge control. The second class of models are based on first principles (Ramadesigan, Northrop, De, Santhanagopalan, Braatz, & Subramanian, 2012). These electrochemical models account for the main underlying physics in the battery, more precisely, they offer an explicit description of the battery dynamics in terms of the main electrochemical parameters and variables. The need for accurate SoC estimation as well as visibility of important electrochemical states and parameters,

☆ A part of this work was carried out during S.-X. Tang's visit to Mitsubishi Electric Research Laboratories, USA. The material in this paper was partially presented at the 2015 American Control Conference, July 1–3, 2015, Chicago, IL, USA. This paper was recommended for publication in revised form by Associate Editor Yoshihiko Miyasato under the direction of Editor Thomas Parisini.

E-mail addresses: sht015@ucsd.edu (S.-X. Tang), lcamacho@ucsd.edu (L. Camacho-Solorio), yebinwang@ieee.org (Y. Wang), krstic@ucsd.edu (M. Krstic).

http://dx.doi.org/10.1016/j.automatica.2017.06.030
0005-1098/

specially in high power and high energy applications, motivates the study of estimation based on electrochemical models.

The widely studied electrochemical Doyle–Fuller–Newman (DFN) model has been shown to accurately describe the main phenomena in lithium-ion batteries (Chaturvedi et al., 2010; Doyle, Fuller, & Newman, 1993). However, the complexity of the model is too high for online SoC estimation (Klein, Chaturvedi, Christensen, Ahmed, Findeisen, & Kojic, 2013). Among the various approximations to the DFN model, the SPM (Guo, Sikha, & White, 2011; Haran, Popov, & White, 1998) is commonly used to derive online SoC estimation algorithms (Moura, Chaturvedi, & Krstic, 2014). In the SPM, diffusion of lithium ions in each electrode is simplified as diffusion in a single spherical particle and electrolyte concentration is assumed to be constant. Still, the SPM has several limitations, for example, being accurate only at low currents (Chaturvedi et al., 2010). Another limitation is that the SPM is restricted to the cases with small variation in internal temperature, which comes from the fact that SPM ignores the dependence of the battery parameters on temperature. In fact, lithium-ion batteries meet issues such as an increase in internal resistance and decrease of capacity, as functions of battery internal average temperature (Guo et al., 2011; Thomas, Newman, & Darling, 2002).

1.3. Estimation algorithms

Extensive efforts have been devoted to developing SoC estimation algorithms, for example, Extended Kalman Filters (EKFs) for ECMs (Plett, 2004) and for the SPM (Santhanagopalan & White, 2006). Estimation algorithms have also been derived for reduced electrochemical models with temperature dynamics, e.g., a linear observer derived to satisfy the conservation of lithium ions (Klein et al., 2013) and a linear observer using pole placement (Tanim, Rahn, & Wang, 2015). These estimation algorithms, together with others based on the unscented Kalman filter or particle filters, rely on some discretization of the diffusion phenomena.

Discretization generally implies a trade-off between high accuracy of the approximation, i.e., a large number of states, and a small number of tuning gains in the observer, i.e. a small number of states. The backstepping approach can be employed to design boundary observers for PDEs in which the discretization is not required. The readers can refer to Smyshlyaev & Krstic (2003) for a preliminary example of boundary observer design for diffusion PDEs via backstepping. This method has been used for the stabilization of various unstable PDE systems, see the tutorial book (Krstic & Smyshlyaev, 2008), in which backstepping boundary controllers and observers are designed for some unstable parabolic, hyperbolic PDEs and other types of PDEs. It has also been applied for stabilizing some coupled PDE–ODE systems (Tang & Xie, 2011a,2011b).

1.4. Contribution

The main contribution of this paper is the derivation of a linear observer for SoC estimation from a simplified thermal–electrochemical model of lithium-ion batteries, i.e., a coupled ODE–PDE model composed by the SPM and a model for the averaged internal temperature (Guo et al., 2011; Tang, Wang, Sahinoglu, Wada, Hara, & Krstic, 2015). Adding thermal dynamics to SPM serves a two-fold purpose: improving the accuracy of SoC estimation and keeping track of the average temperature which is a critical variable for safety management in lithium-ion batteries.

The observer is designed following the PDE backstepping method. It is worth noting that backstepping observers have not been introduced to the problem of battery SoC estimation until very recently (Moura et al., 2014), and by this means the discretization of the diffusion PDEs in the model is avoided. We consider the result presented in this paper as an additional step in the efforts to design estimation and control algorithms for lithium-ion batteries from electrochemical models without relying on the discretization of the PDEs in these models. The main technical challenges in our design consist of proving the well-posedness of the kernel function system for the backstepping transformation. The fact that some coefficients in the thermal–electrochemical model system are time-varying results in a kernel function system with time-varying coefficients, for which the well-posedness is non-trivial to derive. This paper is a continuation of a previous result for SoC estimation from a thermal–electrochemical model of lithium-ion batteries in Tang et al. (2015).

1.5. Organization

The rest of this paper is organized as follows. In Section 2, a temperature-compensated SPM model is presented; and the corresponding SoC estimation problem is formulated in Section 3. In Section 4, a linear observer is developed for estimation of the lithium concentration in the electrodes through boundary state measurements via the backstepping method. The observer error system is proved to be exponentially stable with an arbitrarily designated decay rate, for which the well-posedness is derived by making use of the abstract evolution equation theory. It is worth noting that solving the kernel function system for the backstepping transformation is not trivial because of its dependence on the temperature (Izadi & Dubljevic, 2015; Smyshlyaev & Krstic, 2005). Under some more relaxed assumptions and simplifications than those in Tang et al. (2015), the existence and regularity of the solution to the system are proved in this section. The SoC estimation accuracy is verified by the numerical simulation results presented in Section 5. Finally, some concluding remarks and possible future research topics are given in Section 6.

2. SPM-T model

In this section, the working mechanism of lithium-ion batteries is briefly introduced through an overview of the DFN model. Then, the single particle model with temperature dynamics (Guo et al., 2011; Tang et al., 2015), named SPM-T model, is presented for the purpose of SoC estimation, which can be viewed either as a simplification of the DFN model or as temperature-compensated SPM.

2.1. Working principles of lithium-ion batteries

A lithium-ion battery cell consists of three main regions: negative electrode, separator and positive electrode; all of them characterized by a porous structure. Each electrode includes active materials, conductive fillers, a current collector and a binder. The porous structure of the electrodes provides a large surface area and small distances between lithium ions and active material surfaces for reactions to occur. The separator is placed between the negative and positive electrodes to forbid the flow of electrons between two electrodes while allowing the movement of lithium ions dissolved in the electrolyte. The active materials, intercalated in the lattices of the corresponding electrode, are insertion compounds, i.e. these are host structures in which lithium can be reversibly inserted or extracted. Electrolyte fills all remaining parts of the battery.

The DFN model is derived based on the porous structure all through the lithium-ion battery (Chaturvedi et al., 2010; Thomas et al., 2002). In the DFN model, each electrode is viewed as superposition of active materials, inert filler and electrolyte; justified by the porous configuration. As depicted in Fig. 1, all intercalation particles are assumed to be spheres with a uniform, averaged radius, and the battery is formulated as a pseudo two-dimensional model. The first dimension represents the path along the spatial direction

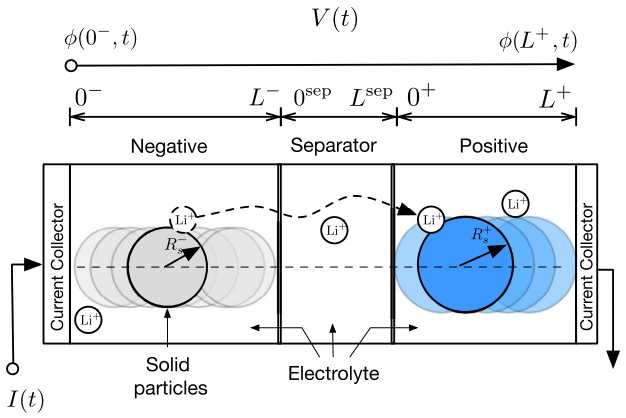

Fig. 1. DFN schematic.

x from the anode, through the separator, to the cathode; and the second dimension is a radial direction r_s used to represent the intercalation and diffusion of lithium ions in the active materials (see Table 1).

Lithium ions move from the negative electrode to the positive electrode during discharging and in the opposite direction during charging. Lithium concentration in the solid phase, i.e. concentration of lithium ions in the active materials, follows the Fick's law of diffusion:

$$\frac{\partial c_s^{\pm}}{\partial t}(t,x,r_s) = \frac{1}{r_s^2}\frac{\partial}{\partial r_s}\left[D_s^{\pm}(T(t))r_s^2\frac{\partial c_s^{\pm}}{\partial r_s}(t,x,r_s)\right], \quad t>0,\ x\in\left(0^{\pm},L^{\pm}\right),\ r_s\in\left(0,R_s^{\pm}\right), \tag{1}$$

$$\frac{\partial c_s^{\pm}}{\partial r_s}(t,x,0) = 0,\ t>0,\ x\in\left(0^{\pm},L^{\pm}\right), \tag{2}$$

$$\frac{\partial c_s^{\pm}}{\partial r_s}(t,x,R_s^{\pm}) = -\frac{1}{D_s^{\pm}(T(t))}j^{\pm}(t,x),\ t>0, x\in\left(0^{\pm},L^{\pm}\right), \tag{3}$$

$$c_s^{\pm}(0,x,r_s) = c_{s0}^{\pm}(x,r_s),\ x\in\left[0^{\pm},L^{\pm}\right], r_s\in\left[0,R_s^{\pm}\right], \tag{4}$$

where the temporal variable is t, the spatial variables are x and r_s. The states of the PDE model (1)–(4) are $c_s^{\pm}(t,x,r_s)\in\mathbb{R}$; the solid phase lithium concentration. The molar fluxes $j^{\pm}(t,x)$ are related to the reaction overpotential $\eta^{\pm}(t,x)$ by the Butler–Volmer equation

$$j^{\pm}(t,x) = \frac{i_0^{\pm}(t,x)}{F}\left[e^{\frac{\alpha_a F}{RT(t)}\eta^{\pm}(t,x)} - e^{-\frac{\alpha_c F}{RT(t)}\eta^{\pm}(t,x)}\right].$$

The reaction overpotentials $\eta^{\pm}(t,x)$ are computed from

$$\eta^{\pm}(t,x) = \phi_s^{\pm}(t,x) - \phi_e^{\pm}(t,x) - U^{\pm}(c_{ss}^{\pm}(t,x),T(t)) - FR_f^{\pm}(T(t))j^{\pm}(t,x).$$

Lithium concentration in the liquid phase $c_e(t,x)$, i.e. concentration of lithium ions in the electrolyte, satisfies the diffusion equation

$$\frac{\partial c_e}{\partial t}(t,x) = \frac{\partial}{\partial x}\left[D_e\frac{\partial c_e}{\partial x}(t,x) + \frac{1-t_c^0}{\varepsilon_e F}i_e(t,x)\right]. \tag{5}$$

Equations for solid electric potential $\phi_s(t,x)$ and electrolyte electric potential $\phi_e(t,x)$ are

$$\frac{\partial \phi_s}{\partial x}(t,x) = \frac{i_e(t,x)-I(t)}{\sigma}, \tag{6}$$

$$\frac{\partial \phi_e}{\partial x}(t,x) = -\frac{i_e(t,x)}{\kappa} + \frac{2RT(t)}{F}(1-t_c^0)\left(1+\frac{\mathrm{d}\ln f_{c/a}}{\mathrm{d}\ln c_e}(t,x)\right)\frac{\partial \ln c_e}{\partial x}(t,x), \tag{7}$$

Table 1
Nomenclature.

Variables	
c_s	Lithium concentration in the solid phase
c_{ss}	Lithium concentration at the surface of the particle
c_e	Constant lithium concentration in the electrolyte
$\bar{c}_s$	Volume averaged lithium concentration in the solid phase
j	Molar flux of lithium at the surface of the particle
ϕ_s	Electric potential in the solid phase
ϕ_e	Electric potential in the electrolyte
η	Reaction overpotential
U	Open-circuit potential
i_0	Exchange current density
i_e	Electrolyte current density normalized by cross-sectional area
T	Internal average temperature
T_{amb}	Ambient temperature
I	External current density normalized by cross-sectional area
V	Terminal voltage
$\bar{q}_s$	Volume averaged flux
Parameters	
L	Length
D_s	Diffusion coefficient of lithium in the solid phase
D_e	Diffusion coefficient of lithium in the electrolyte
c_s^{max}	Maximum lithium concentration in the solid phase
R_s	Radius of the particle
α_a	Anodic transfer coefficient
α_c	Cathodic transfer coefficient
r_{eff}	Effective reaction rate in the solid phase
R_f	Film resistance of the solid-electrolyte interphase
R_c	Contact resistance between the electrode and current collector
ε_s	Volume fraction of the active material
ε_e	Volume fraction of the electrolyte
a_s	Interfacial surface area
F	Faraday's constant
R	Universal gas constant
$N_{Li,s}$	Total number of lithium ions in the solid phase
σ	Electronic conductivity in the solid phase
κ	Ionic conductivity in the electrolyte
t_c^0	Transference number of the ions w.r.t. the solvent velocity
$f_{c/a}$	Mean molar activity coefficient in the electrolyte
ρ^{avg}	Average density
c_P	Heat capacity
h_{cell}	Heat transfer coefficient
E	Activation energy coefficient
Super- and subscripts	
+	Positive electrode
−	Negative electrode
sep	Separator
s	Solid phase
e	Electrolyte

where $I(t)$ is the external current density normalized by cross-sectional area. Charge conservation in the electrodes provides a relation between electrolyte current densities $i_e^{\pm}(x,t)$ and molar fluxes $j^{\pm}(t,x)$:

$$\frac{\partial i_e^{+}}{\partial x}(t,x) = -a_s^{+}Fj^{+}(t,x),$$

$$\frac{\partial i_e^{-}}{\partial x}(t,x) = a_s^{-}Fj^{-}(t,x),$$

with boundary conditions $i_e^{-}(t,0^-) = i_e^{+}(t,L^+) = 0$ and $i_e^{-}(t,L^-) = i_e^{+}(t,0^+) = I(t)$. In the separator, $i_e(t,x) = I(t)$. Output voltage is the difference between the two solid electric potentials computed as

$$V(t) = \phi_s(t,L^+) - \phi_s(t,0^-).$$

The readers should refer to Chaturvedi et al. (2010) for a complete description of the DFN model and for the boundary conditions for Eqs. (5)–(7). Note that we are using the convention: positive current for discharging and negative current for charging.

2.2. The SPM-T model

The DFN model accurately describes many aspects of the lithium-ion cells working mechanism; however, the complexity of the model is too high for online SoC estimation. For this reason, we present a simplified model which is the single particle model with temperature dynamics, i.e., the SPM-T model. The SPM-T model (Guo et al., 2011; Tang et al., 2015) is derived by making the following assumptions and simplifications:

- concentration of lithium ions in the electrolyte $c_e(t,x)$ is uniform in both time and space,
- molar fluxes $j^{\pm}(t,x)$ are uniform in the x-direction,
- concentration of lithium ions in the active materials $c_s(t,x)$ is uniform in the x-direction.

Moreover, each electrode is modeled as a single spherical particle in this simplification; representative of all particles in the electrode. Compared with the SPM-T model presented in Guo et al. (2011), here we choose not to take into account the electrolyte resistance R_{cell}, i.e., we set $R_{\text{cell}} = 0$ (Klein et al., 2013).

In the coupled SPM-T model, the SPM subsystem is

$$\frac{\partial c_s^{\pm}}{\partial t}(t,r_s) = \frac{1}{r_s^2}\frac{\partial}{\partial r_s}\left[D_s^{\pm}(T(t))r_s^2\frac{\partial c_s^{\pm}}{\partial r_s}(t,r_s)\right], \quad t>0,\ r_s\in(0,R_s^{\pm}), \tag{8}$$

$$\frac{\partial c_s^{\pm}}{\partial r_s}(t,0) = 0,\ t>0, \tag{9}$$

$$\frac{\partial c_s^{\pm}}{\partial r_s}(t,R_s^{\pm}) = -\frac{1}{D_s^{\pm}(T(t))}j^{\pm}(t),\ t>0, \tag{10}$$

$$c_s^{\pm}(0,r_s) = c_{s,0}^{\pm}(r_s),\ r_s\in[0,R_s^{\pm}]. \tag{11}$$

The states of the system (8)–(11) are $c_s^{\pm}(t,r_s)\in\mathbb{R}$, with the temporal variable t and the spatial variables r_s. The relation between molar fluxes $j^{\pm}(t)$ and current $I(t)$ becomes linear:

$$j^{+}(t) = -\frac{I(t)}{a_s^{+}FL^{+}},\ j^{-}(t) = \frac{I(t)}{a_s^{-}FL^{-}}.$$

By assuming the same value to the anodic and cathodic transfer coefficients, i.e., $\alpha \triangleq \alpha_a = \alpha_c$, a simple relation between reaction overpotentials and molar fluxes can be found as

$$\eta^{\pm}(t) = \frac{RT(t)}{\alpha F}\sinh^{-1}\left(\frac{F}{2i_0^{\pm}(t)}j^{\pm}(t)\right),$$

where

$$i_0^{\pm}(t) = r_{\text{eff}}^{\pm}(T(t))\left[c_{ss}^{\pm}(t)\right]^{\alpha_c}\left[c_{e,0}\left(c_s^{\pm,\max}-c_{ss}^{\pm}(t)\right)\right]^{\alpha_a}, \tag{12}$$

with $c_{ss}^{\pm}(t)\triangleq c_s^{\pm}(t,R_s^{\pm})$. The parameter $c_{e,0}$ in Eq. (12) denotes the electrolyte concentration at equilibrium. Solid electric potentials are computed from

$$\phi_s^{\pm}(t) = \eta^{\pm}(t) + U^{\pm}(c_{ss}^{\pm}(t),T(t)) + FR_f^{\pm}(T(t))j^{\pm}(t).$$

Output voltage is now the difference between solid electric potentials in the positive electrode and negative electrode:

$$\begin{aligned} V(t) &= \phi_s^{+}(t) - \phi_s^{-}(t) \\ &= -\frac{RT(t)}{\alpha F}\left[\sinh^{-1}\left(\frac{1}{2i_0^{+}(t)}\frac{I(t)}{a^{+}L^{+}}\right) + \sinh^{-1}\left(\frac{1}{2i_0^{-}(t)}\frac{I(t)}{a^{-}L^{-}}\right)\right] \\ &\quad - \left(\frac{R_f^{+}(T(t))}{a^{+}L^{+}} + \frac{R_f^{-}(T(t))}{a^{-}L^{-}}\right)I(t) \\ &\quad + U^{+}(c_{ss}^{+}(t),T(t)) - U^{-}(c_{ss}^{-}(t),T(t)). \end{aligned} \tag{13}$$

Parameters $D_s^{\pm}(T(t))$, $r_{\text{eff}}^{\pm}(T(t))$ and $R_f^{\pm}(T(t))$ are functions with an Arrhenius-like dependence (Klein et al., 2013) on the battery cell internal average temperature $T(t)$, i.e.,

$$D_s^{\pm}(T(t)) = D_s^{\pm}(T(0))e^{E_{D_s^{\pm}}\frac{T(t)-T(0)}{T(t)T(0)}}, \tag{14}$$

$$r_{\text{eff}}^{\pm}(T(t)) = r_{\text{eff}}^{\pm}(T(0))e^{E_{r_{\text{eff}}^{\pm}}\frac{T(t)-T(0)}{T(t)T(0)}}, \tag{15}$$

$$R_f^{\pm}(T(t)) = R_f^{\pm}(T(0))e^{E_{R_f^{\pm}}\frac{T(t)-T(0)}{T(t)T(0)}}, \tag{16}$$

where $E_{D_s^{\pm}}$, $E_{r_{\text{eff}}^{\pm}}$, $E_{R_f^{\pm}}$, are activation energy coefficients. Internal average temperature satisfies the following ODE (Thomas et al., 2002, Section 12.3.7)

$$\begin{aligned} \rho^{\text{avg}}c_P\frac{dT}{dt}(t) &= h_{\text{cell}}\left(T_{\text{amb}}(t)-T(t)\right) - I(t)V(t) \\ &\quad + I(t)\Big\{U^{+}(\bar{c}_s^{+}(t),T(t)) - U^{-}(\bar{c}_s^{-}(t),T(t)) \\ &\quad - T(t)\left[\frac{\partial U^{+}(\bar{c}_s^{+}(t),T(t))}{\partial T} - \frac{\partial U^{-}(\bar{c}_s^{-}(t),T(t))}{\partial T}\right]\Big\} \\ &\quad + R_cI(t)^2,\ t>0, \end{aligned} \tag{17}$$

$$T(0) = T_{\text{amb}}(0), \tag{18}$$

where $\bar{c}_s^{\pm}(t)$ are the average concentrations defined as

$$\bar{c}_s^{\pm}(t) = \frac{3}{(R_s^{\pm})^3}\int_0^{R_s^{\pm}} r_s^2c_s^{\pm}(t,r_s)dr_s.$$

The system states are the solid phase lithium ion concentrations $c_s^{\pm}(t,r_s)\in\mathbb{R}$ in the PDE (8)–(11) and the internal average temperature $T(t)$ in the ODE (17)–(18).

3. Problem formulation

3.1. Estimation objective

Our objective is to estimate the battery SoC, defined as the normalized averaged lithium concentration in the negative electrode, i.e.,

$$\text{SoC}(t) = \frac{3}{(R_s^{-})^3}\int_0^{R_s^{-}} r_s^2\frac{c_s^{-}(t,r_s)}{c_{s,\max}^{-}}dr_s = \frac{\bar{c}_s^{-}(t)}{c_{s,\max}^{-}}, \tag{19}$$

from measurements of the input current $I(t)$ and the output voltage $V(t)$. For this purpose, boundary observers can be constructed to estimate the concentrations of lithium ions in the electrodes $c_s^{-}(t,r_s)$ by using the boundary values, i.e., the corresponding surface concentrations $c_{ss}^{-}(t)$. Note however that in (13), boundary values $c_{ss}^{-}(t)$ are not directly available from measurement of $V(t)$. Instead, they appear in $V(t)$ with a nonlinear fashion, i.e., the nonlinearities within the exchange current densities $i_0^{-}(t)$ and within the subtraction between the nonlinear Open-Circuit Potential (OCP) functions $U^{-}(t,c_{ss}^{-}(t))$. Therefore, in order to overcome the lack of boundary value measurements required by the boundary observers, an inversion of the output function $V(t)$ with respect to the boundary values is needed.

To ease inversion of the output voltage, the lithium concentration dynamics in one of the electrodes will be simplified. Inversion will then be done with respect to the surface concentration of the electrode with unsimplified lithium concentration dynamics. The leading terms in the output voltage are the OCP functions and we are assuming that the OCP functions are invertible with respect to the surface concentration in the corresponding unsimplified electrode. In this paper, we will simplify the lithium concentration dynamics in the negative electrode and invert the output function with respect to the surface concentration in the positive electrode, and a boundary observer will then be derived for estimation of lithium ion concentration in the positive electrode.

Remark 1. The decision of simplifying the negative electrode dynamics instead of the positive one is made based on the sensitivity of OCPs to surface concentrations. For some common lithium ion active materials, $\partial U^+/\partial c_{ss}^+$ is larger that $\partial U^+/\partial c_{ss}^-$ in magnitude, thus making it easier to recover c_{ss}^+ from the voltage measurement $V(t)$.

One can easily prove that the total amount of lithium ions in solid phase $N_{Li,s}$ is conserved (Klein et al., 2013), i.e.,

$$\frac{dN_{Li,s}}{dt} = 0, \tag{20}$$

where

$$N_{Li,s} = \varepsilon^+ L^+ \bar{c}_s^+(t) + \varepsilon^- L^- \bar{c}_s^-(t).$$

Since we assume $N_{Li,s}$ is a known quantity, i.e. a parameter in the model, then we can also compute the battery SoC in the negative electrode from the averaged lithium concentration in the positive electrode, i.e.

$$\text{SoC}(t) = \frac{N_{Li,s} - \varepsilon^+ L^+ \bar{c}_s^+(t)}{\varepsilon^- L^- c_{s,\max}^-}. \tag{21}$$

3.2. Output function inversion

The goal of the output function inversion is to write $V(t)$ as a function of only of $c_{ss}^+(t)$ and $I(t)$.

3.2.1. Write $V(t)$ as a function of $c_{ss}^{\pm}(t)$, $\bar{c}_s^{\pm}(t)$ and $I(t)$

The first step is to simplify the internal average temperature dynamics to derive an expression for $T(t)$ only in terms of time and current, i.e., a time-varying function $\check{T}(t) \triangleq \check{T}(t, I(t), T_{amb}(t))$ independent of the concentrations $c_s^{\pm}(t)$, $c_{ss}^{\pm}(t)$. We start by substituting the output voltage equation (13) into the original average temperature equation (17):

$$\begin{aligned}
\rho^{avg} c_P \frac{dT}{dt}(t) &= h_{cell}\,(T_{amb}(t) - T(t)) \\
&+ I(t)\frac{RT(t)}{\alpha F}\left[\sinh^{-1}\left(\frac{1}{2i_0^+(t)}\frac{I(t)}{a^+L^+}\right) + \sinh^{-1}\left(\frac{1}{2i_0^-(t)}\frac{I(t)}{a^-L^-}\right)\right] \\
&+ \left(\frac{R_f^+(T(t))}{a^+L^+} + \frac{R_f^-(T(t))}{a^-L^-} - R_c\right) I(t)^2 \\
&- I(t)\left[U^+(c_{ss}^+(t), T(t)) - U^-(c_{ss}^-(t), T(t))\right] \\
&+ I(t)\Bigg\{U^+(\bar{c}_s^+(t), T(t)) - U^-(\bar{c}_s^-(t), T(t)) \\
&- T(t)\left[\frac{\partial U^+(\bar{c}_s^+(t), T(t))}{\partial T} - \frac{\partial U^-(\bar{c}_s^-(t), T(t))}{\partial T}\right]\Bigg\}.
\end{aligned} \tag{22}$$

We assume that the functions $U^{\pm}(\cdot, T(t))$ and $i_0^{\pm}(\cdot)$ are independent of concentrations but possibly time-varying, and we replace their dependence on temperature $T(t)$ with dependence on the ambient temperature $T_{amb}(t)$. For this purpose, denote

$$\begin{aligned}
\check{U}_1^{\pm}(t) &\triangleq U^{\pm}(c_{ss}^{\pm}(t), T_{amb}(t)), \\
\check{U}_2^{\pm}(t) &\triangleq U^{\pm}(\bar{c}_s^{\pm}(t), T_{amb}(t)), \\
\check{i}_0^{\pm}(t) &\triangleq i_0^{\pm}(T_{amb}(t)),
\end{aligned}$$

where subscript 1 in $\check{U}$ is used to denote the approximation of $U^{\pm}(\cdot, T(t))$ when they are evaluated at the surface concentration and subscript 2 when they are evaluated at the averaged concentration. Similarly, for the temperature dependent parameters $R_f^{\pm}(T(t))$ and $r_{eff}^{\pm}(T(t))$, we also replace dependence on $T(t)$ with $T_{amb}(t)$, i.e.,

$$\begin{aligned}
\check{r}_{eff}^{\pm}(t) &\triangleq r_{eff}^{\pm}(T_{amb}(t)), \\
\check{R}_f^{\pm}(t) &\triangleq R_f^{\pm}(T_{amb}(t)).
\end{aligned}$$

Thus, we can rewrite Eq. (22) as

$$\rho^{avg} c_P \frac{d\check{T}}{dt}(t) = \chi(t)\check{T}(t) + \omega(t), \tag{23}$$

where

$$\begin{aligned}
\chi(t) = &- h_{cell} + \frac{R}{\alpha F} I(t)\Bigg[\sinh^{-1}\left(\frac{1}{2\check{i}_0^+(t)}\frac{I(t)}{a^+L^+}\right) \\
&+ \sinh^{-1}\left(\frac{1}{2\check{i}_0^-(t)}\frac{I(t)}{a^-L^-}\right)\Bigg] \\
&- I(t)\left[\frac{\partial \check{U}_2^+}{\partial T}(t) - \frac{\partial \check{U}_2^-}{\partial T}(t)\right], \\
\omega(t) = &\, h_{cell} T_{amb}(t) + \left(\frac{\check{R}_f^+(t)}{a^+L^+} + \frac{\check{R}_f^-(t)}{a^-L^-} - R_c\right) I(t)^2 \\
&- I(t)\left[\check{U}_1^+(t) - \check{U}_1^-(t)\right] + I(t)\left[\check{U}_2^+(t) - \check{U}_2^-(t)\right],
\end{aligned}$$

then, it holds that

$$\begin{aligned}
\check{T}(t) = &\, \check{T}(0) e^{\frac{1}{\rho^{avg} c_P}\int_0^t \chi(\tau)d\tau} \\
&+ \frac{1}{\rho^{avg} c_P}\int_0^t e^{\frac{1}{\rho^{avg} c_P}\int_0^{t-\tau}\chi(\sigma)d\sigma}\omega(\tau)d\tau.
\end{aligned} \tag{24}$$

Substituting (24) into (13) yields the following simplified output function:

$$\begin{aligned}
V(t) = &- \frac{R\check{T}(t)}{\alpha F}\left[\sinh^{-1}\left(\frac{1}{2i_0^+(t)}\frac{I(t)}{a^+L^+}\right)\right. \\
&\left. + \sinh^{-1}\left(\frac{1}{2i_0^-(t)}\frac{I(t)}{a^-L^-}\right)\right] \\
&- \left(\frac{R_f^+(\check{T}(t))}{a^+L^+} + \frac{R_f^-(\check{T}(t))}{a^-L^-}\right) I(t) \\
&+ U^+(c_{ss}^+(t), \check{T}(t)) - U^-(c_{ss}^-(t), \check{T}(t)), \\
\triangleq &\, h_1(t, c_{ss}^{\pm}(t), \bar{c}_s^{\pm}(t), I(t)).
\end{aligned} \tag{25}$$

3.2.2. Write $V(t)$ as a function of $c_{ss}^+(t)$ and $I(t)$

In order to further simplify the output function, we are to establish relations between $c_{ss}^+(t)$ and the other concentrations $c_{ss}^-(t)$, $\bar{c}_s^+(t)$, $\bar{c}_s^-(t)$. Consider the following approximate polynomial solution profiles of the electrode diffusion dynamics (Subramanian, Diwakar, & Tapriyal, 2005)[1]:

$$\bar{c}_s^{\pm}(t) = c_{ss}^{\pm}(t) - \frac{8R_s^{\pm}}{35}\bar{q}_s^{\pm}(t) + \frac{R_s^{\pm}}{35D_s^{\pm}(\check{T}(t))} j^{\pm}(t), \tag{26}$$

where the volume averaged fluxes $\bar{q}_s^{\pm}(t)$ satisfy

$$\frac{d}{dt}\bar{q}_s^{\pm}(t) = -\frac{30D_s^{\pm}(\check{T}(t))}{(R_s^{\pm})^2}\bar{q}_s^{\pm}(t) - \frac{45}{2(R_s^{\pm})^2} j^{\pm}(t).$$

Moreover, from the conservation (20) of lithium ions in solid phase $N_{Li,s}$, we can write the relation

$$\bar{c}_s^-(t) = \alpha \bar{c}_s^+(t) + \beta, \tag{27}$$

[1] Note that (26) is obtained by assuming the following polynomial solution profile

$$\begin{aligned}
c_s^{\pm}(t, r) = &\frac{39}{4}c_{ss}^{\pm}(t) - 3\bar{q}_s^{\pm}(t)R_s^{\pm} - \frac{35}{4}\bar{c}_s^{\pm}(t) \\
&+ \left(-35c_{ss}^{\pm}(t) + 10\bar{q}_s^{\pm}(t)R_s^{\pm} + 35\bar{c}_s^{\pm}(t)\right)\frac{(r_s^{\pm})^2}{(R_s^{\pm})^2} \\
&+ \left(\frac{105}{4}c_{ss}^{\pm}(t) - 7\bar{q}_s^{\pm}(t)R_s^{\pm} - \frac{105}{4}\bar{c}_s^{\pm}(t)\right)\frac{r_s^4}{(R_s^{\pm})^4}.
\end{aligned}$$

where $\alpha = -\frac{\varepsilon^+ L^+}{\varepsilon^- L^-}$ and $\beta = \frac{N_{\text{Li,s}}}{\varepsilon^- L^-}$. It then immediately follows from (26) and (27) that

$$\bar{c}_s^-(t) = \alpha\left(c_{ss}^+(t) - \frac{8R_s^+}{35}\bar{q}_s^+(t) + \frac{R_s^+}{35D_s^+(\check{T}(t))}j^+(t)\right) + \beta, \tag{28}$$

and

$$\begin{aligned} c_{ss}^-(t) &= \bar{c}_s^-(t) + \frac{8R_s^-}{35}\bar{q}_s^-(t) - \frac{R_s^-}{35D_s^-(\check{T}(t))}j^-(t) \\ &= \alpha\left(c_{ss}^+(t) - \frac{8R_s^+}{35}\bar{q}_s^+(t) + \frac{R_s^+}{35D_s^+(\check{T}(t))}j^+(t)\right) + \beta \\ &\quad + \frac{8R_s^-}{35}\bar{q}_s^-(t) - \frac{R_s^-}{35D_s^-(\check{T}(t))}j^-(t). \end{aligned} \tag{29}$$

Therefore, from (25), (26), (28) and (29), we obtain a further simplified version of the output function:

$$V(t) = h_2(t, c_{ss}^+(t), I(t)). \tag{30}$$

3.2.3. Inversion of the function h_2

As long as the function (30) is a one-to-one correspondence w.r.t. $c_{ss}^+(t)$, uniformly in $I(t)$, one could invert it to derive the boundary concentration in the positive electrode as

$$c_{ss}^+(t) = h_0(t, V(t), I(t)).$$

3.3. Normalization and state transformation

We perform normalization and state transformation to simplify the system and thus also the structure of to-be-designed observer. Let $r = r_s/R_s^+$ for normalization and proceed the state transformation $c(t, r) = r_s c_s^+(t, r_s)$, then the PDE subsystem (8)–(11) is transformed into[2]

$$\frac{\partial c}{\partial t}(t, r) = \frac{D_s^+(\check{T}(t))}{(R_s^+)^2}\frac{\partial^2 c}{\partial r^2}(t, r),\ t > 0,\ r \in (0, 1), \tag{31}$$

$$c(t, 0) = 0,\ t > 0, \tag{32}$$

$$\frac{\partial c}{\partial r}(t, 1) - c(t, 1) = \frac{R_s^+}{D_s^+(\check{T}(t))}\frac{I(t)}{a^+FL^+} \triangleq I_1(t),\ t > 0, \tag{33}$$

$$c(0, r) = c_0(r) = R_s^+ r c_s^+(0, R_s^+ r),\ r \in [0, 1]. \tag{34}$$

Our objective now is to design an observer for this normalized and transformed PDE system.

4. Backstepping state observer

With the inversion of the output function in Section 3.2, the boundary concentration in the positive electrode is then available for observer design. Again, we assume that the internal averaged temperature is a time-varying and concentration-independent function which can be computed from the simplified Eq. (24). Thus, the function $D_s^+(\check{T}(t))$ will be treated as known. Moreover, assume that $I(t)$, $U^{\pm}(\cdot, \check{T}(t))$ and $V(t)$ are piecewise (real) analytic. In what follows, we only consider the proof piecewisely so that both $I(t)$ and $V(t)$ are analytic in each separate time interval. Then, from (24) and with the assumption that $\partial U^{\pm}/\partial T$ are also analytic in each corresponding time interval, we can prove by induction that the nth order derivative of $\check{T}(t)$ is differentiable for any nonnegative integer n. Further, we can derive that $\check{T}(t)$ is analytic in each time interval. Without loss of generality, consider $t \in [0, t_{\max}]$ where $t_{\max}$ is an appropriate finite time for the regularities to hold.

A Luenberger-type observer for the normalized and transformed PDE system (31)–(34) can be designed:

$$\frac{\partial \hat{c}}{\partial t}(t, r) = \frac{D_s^+(\check{T}(t))}{(R_s^+)^2}\frac{\partial^2 \hat{c}}{\partial r^2}(t, r) + p_1(t, r)(c(t, 1) - \hat{c}(t, 1)),\ t > 0,\ r \in (0, 1), \tag{35}$$

$$\hat{c}(t, 0) = 0,\ t > 0, \tag{36}$$

$$\frac{\partial \hat{c}}{\partial r}(t, 1) - \hat{c}(t, 1) = I_1(t) + p_{10}(t)(c(t, 1) - \hat{c}(t, 1)),\ t > 0, \tag{37}$$

$$\hat{c}(0, r) = \hat{c}_0(r),\ r \in [0, 1], \tag{38}$$

which is a copy of the plant together with output error injection terms. Here, $\hat{c}_0(r)$ denotes the initial condition of the observer, and the boundary state error injection gains $p_1(t, r)$ and $p_{10}(t)$ are to be determined to guarantee the stability of the estimation error system

$$\frac{\partial \tilde{c}}{\partial t}(t, r) = \frac{D_s^+(\check{T}(t))}{(R_s^+)^2}\frac{\partial^2 \tilde{c}}{\partial r^2}(t, r) - p_1(t, r)\tilde{c}(t, 1),\ t > 0,\ r \in (0, 1), \tag{39}$$

$$\tilde{c}(t, 0) = 0, \tag{40}$$

$$\frac{\partial \tilde{c}}{\partial r}(t, 1) - \tilde{c}(t, 1) = -p_{10}(t)\tilde{c}(t, 1), \tag{41}$$

$$\tilde{c}(0, r) = c_0(r) - \hat{c}_0(r) \triangleq \tilde{c}_0(r), \tag{42}$$

with $\tilde{c}(t, r) \triangleq c(t, r) - \hat{c}(t, r)$. In order to find the output injection gains, the PDE backstepping method (Krstic & Smyshlyaev, 2008) is employed. We would like to find an invertible transformation

$$\tilde{c}(t, r) = \tilde{w}(t, r) - \int_r^1 p(t, r, \iota)\tilde{w}(t, \iota)\mathrm{d}\iota \tag{43}$$

so that $\tilde{w}$ satisfies the following exponentially stable target system:

$$\frac{\partial \tilde{w}}{\partial t}(t, r) = \frac{D_s^+(\check{T}(t))}{(R_s^+)^2}\frac{\partial^2 \tilde{w}}{\partial r^2}(t, r) + \lambda\tilde{w}(t, r), \tag{44}$$

$$\tilde{w}(t, 0) = 0, \tag{45}$$

$$\frac{\partial \tilde{w}}{\partial r}(t, 1) = -\frac{1}{2}\tilde{w}(t, 1), \tag{46}$$

$$\tilde{w}(0, r) = \tilde{w}_0(r), \tag{47}$$

where $\tilde{w}_0(r)$ denotes the initial condition to be determined for the target system, and $\lambda < \min_{t\geq 0}\{D_s^-(\check{T}(t))\}/(4(R_s^+)^2)$ is a free parameter to be chosen, which determines the convergence rate of the observer state in (39)–(42) to the system state in (31)–(34). The following lemma states the exponential stability of the $\tilde{w}$-system (44)–(47).

Lemma 2. *Let $t \in [0, t_{\max}]$. If*

$$\lambda < \frac{1}{4(R_s^-)^2}\min_{t\geq 0}\{D_s^+(\check{T}(t))\}, \tag{48}$$

then for any initial data $\tilde{w}_0(\cdot) \in L^2(0, 1)$, the $\tilde{w}$-system (44)–(47) admits a (mild) solution $\tilde{w}(t, \cdot) \in L^2(0, 1)$ and is exponentially stable at $\tilde{w} \equiv 0$. Moreover, if the boundary compatibility condition is satisfied, the solution is classical.

Proof. Consider the state space $\boldsymbol{H} = L^2(0, 1)$. For every $t \in [0, t_{\max}]$, define a linear operator $\mathcal{A}(t) : \mathrm{Dom}(\mathcal{A}(t)) \subset \boldsymbol{H} \to \boldsymbol{H}$

[2] The normalization transformation $\bar{t} = D_s^+(\check{T}(t))/(R_s^+)^2 t$ employed in Moura et al. (2014) is not used in this paper. The reason is that $T(t)$ is not known a priori in this case, needing to be measured or derived at each time step. Thus, the corresponding inverse transformation cannot be trivially obtained.

as follows:

$$\mathcal{A}(t)\varphi = \frac{D_s^+(\check{T}(t))}{(R_s^+)^2}\varphi'' + \lambda\varphi, \quad \forall\varphi \in \mathrm{Dom}(\mathcal{A}(t)),$$
$$\mathrm{Dom}(\mathcal{A}(t)) = \left\{\varphi \in H^2(0,1);\ \varphi(0) = 0,\ \varphi'(1) = -\frac{1}{2}\varphi(1)\right\}.$$

Then, the system (44)–(47) can be written into the following abstract equation:

$$\frac{\mathrm{d}}{\mathrm{d}t}\tilde{w}(t,\cdot) = \mathcal{A}(t)\tilde{w}(t,\cdot),\ 0 \le t \le t_{\max}, \tag{49}$$
$$\tilde{w}(0,\cdot) = \tilde{w}_0(\cdot). \tag{50}$$

Note that $\mathrm{Dom}(\mathcal{A}(t))$ is dense in $\boldsymbol{H}$ and independent of t, and it can be proved that $\mathcal{A}(t)$ is for each t the infinitesimal generator of an exponential stable semigroup. Indeed, all the assumptions (P1)–(P3) in Pazy (1983, Section 5.6) are satisfied. Thus, from Pazy (1983, Section 5.6, Theorem 6.1), there exists a unique evolution system corresponding to (49)–(50) and (44)–(47) as well. Furthermore, by considering the Lyapunov function $V(t) = \frac{1}{2}\|\tilde{w}(t,\cdot)\|^2_{L^2(0,1)}$, we get

$$\begin{aligned}\dot{V}(t) &= \int_0^1 \tilde{w}(t,r)\left[\frac{D_s^+(\check{T}(t))}{(R_s^+)^2}\frac{\partial^2\tilde{w}}{\partial r^2}(t,r) + \lambda\tilde{w}(t,r)\right]\mathrm{d}r\\ &= \frac{D_s^+(\check{T}(t))}{(R_s^+)^2}\left[-\frac{1}{2}\tilde{w}^2(t,1) - \|\tilde{w}_r(t,\cdot)\|^2_{L^2(0,1)}\right]\\ &\quad + \lambda\|\tilde{w}(t,\cdot)\|^2_{L^2(0,1)}\\ &\le -2\left(\frac{D_s^+(\check{T}(t))}{4(R_s^+)^2} - \lambda\right)V(t),\end{aligned} \tag{51}$$

where (44) is used in the first line, (45), (46) and integration by parts are applied in the second line, and the Poincaré Inequality (Krstic & Smyshlyaev, 2008, Lemma 2.1)

$$\|\tilde{w}(t,\cdot)\|^2_{L^2(0,1)} \le 4\|\tilde{w}_r(t,\cdot)\|^2_{L^2(0,1)}$$

is employed in the last line. As a result, from (48), exponential stability of the $\tilde{w}$-system (44)–(47) is proved. □

For notation simplicity we will denote the $L^2(0,1)$-norm by $\|\cdot\|$ in the sequel.

Differentiating the transformation (43) with respect to t gives

$$\begin{aligned}\tilde{c}_t(t,r) &= \frac{D_s^+(\check{T}(t))}{(R_s^+)^2}\Bigg[\frac{\partial^2\tilde{w}}{\partial r^2}(t,r) + p(t,r,r)\tilde{w}_r(t,r)\\ &\quad + \left(p_\iota(t,r,1) + \frac{1}{2}p(t,r,1)\right)\tilde{w}(t,1)\Bigg]\\ &\quad + \left[\lambda - \frac{D_s^+(\check{T}(t))}{(R_s^+)^2}p_\iota(t,r,r)\right]\tilde{w}(t,r)\\ &\quad - \int_r^1\Bigg[p_t(t,r,\iota) + \lambda p(t,r,\iota)\\ &\quad + \frac{D_s^+(\check{T}(t))}{(R_s^+)^2}p_\iota(t,r,\iota)\Bigg]\tilde{w}(t,\iota)\mathrm{d}\iota,\end{aligned} \tag{52}$$

where (44), (46) and integration by parts have been used in the calculation. Differentiating (43) with respect to r gives

$$\begin{aligned}\tilde{c}_r(t,r) &= \tilde{w}_r(t,r) + p(t,r,r)\tilde{w}(t,r)\\ &\quad - \int_r^1 p_r(t,r,\iota)\tilde{w}(t,\iota)\mathrm{d}\iota,\end{aligned} \tag{53}$$

$$\begin{aligned}\tilde{c}_{rr}(t,r) &= \tilde{w}_{rr}(t,r) + p(t,r,r)\tilde{w}_r(t,r)\\ &\quad + \left(\frac{\mathrm{d}}{\mathrm{d}r}p(t,r,r) + p_r(t,r,r)\right)\tilde{w}(t,r)\\ &\quad - \int_r^1 p_{rr}(t,r,\iota)\tilde{w}(t,\iota)\mathrm{d}\iota.\end{aligned} \tag{54}$$

From (39)–(42), (43), (45)–(47) and (52)–(54), we derive that the kernel function $p(t,r,\iota)$ needs to satisfy the following PDE system:

$$p_t(t,r,\iota) = \frac{D_s^+(\check{T}(t))}{(R_s^+)^2}\left[(p_{rr}(t,r,\iota) - p_{\iota\iota}(t,r,\iota)\right] - \lambda p(t,r,\iota), \tag{55}$$
$$p(t,0,\iota) = 0, \tag{56}$$
$$p(t,r,r) = \frac{(R_s^+)^2}{2D_s^+(\check{T}(t))}\lambda r, \tag{57}$$
$$p(0,r,\iota) = p_0(r,\iota), \tag{58}$$

for which the domain is $\mathcal{T} = \{(t,r,\iota);\ 0 \le t \le t_{\max},\ 0 \le \iota \le r \le 1\}$. Here, $p_0(r,\iota)$ denotes the initial condition for the kernel system and satisfies

$$\int_r^1 p_0(r,\iota)\tilde{w}(t,\iota)\mathrm{d}\iota = c_0(r) - \hat{c}_0(r) - \tilde{w}_0(r). \tag{59}$$

Moreover, the observer gains need to be chosen as

$$p_1(t,r) = -\frac{D_s^+(\check{T}(t))}{(R_s^+)^2}\left(p_\iota(t,r,1) + \frac{1}{2}p(t,r,1)\right), \tag{60}$$
$$p_{10}(t) = \frac{3}{2} - \frac{(R_s^+)^2}{2D_s^+(\check{T}(t))}\lambda. \tag{61}$$

In more detail, first, plugging (43), (52) and (54) into (39) gives (55), (60) and the boundary condition

$$\frac{\mathrm{d}}{\mathrm{d}r}p(t,r,r) = \frac{(R_s^+)^2}{2D_s^+(\check{T}(t))}\lambda. \tag{62}$$

Second, plugging (40) and (45) into (43) gives (56). Third, (57) is derived from (62) and (56). Then, (61) is derived from (41), (43), (46), (53) and (57). Finally, (59) is derived by plugging (42) and (47) into (43).

4.1. Well-posedness of the kernel function $p(r,\iota,t)$

Lemma 3. *The initial data $p_0(\cdot,\cdot)$ is an analytic function in $\mathbb{T} = \{(r,\iota);\ 0 \le \iota \le r \le 1\}$, and the system (55)–(58) admits an analytic solution $p(t,\cdot,\cdot)$ in $\mathcal{T}$.*

Proof. ***We first transform the system (55)–(58) into an equivalent integral equation.*** Let $\xi = r+\iota$, $\eta = r-\iota$ and $q(t,\xi,\eta) = p(t,r,\iota)$, then we have from (55)–(58) that q satisfies the following PDE:

$$q_t(t,\xi,\eta) = 4\frac{D_s^+(\check{T}(t))}{(R_s^+)^2}q_{\xi\eta}(t,\xi,\eta) - \lambda q(t,\xi,\eta), \tag{63}$$
$$q(t,\xi,-\xi) = 0, \tag{64}$$
$$q(t,\xi,0) = \frac{(R_s^+)^2}{4D_s^+(\check{T}(t))}\lambda\xi, \tag{65}$$

with the initial condition

$$q(0,\xi,\eta) = p\left(0,\frac{\xi+\eta}{2},\frac{\xi-\eta}{2}\right).$$

Eq. (63) can be rewritten as

$$q_{\xi\eta}(t,\xi,\eta)=\frac{(R_s^+)^2}{4D_s^+(\check{T}(t))}\left(q_t(t,\xi,\eta)+\lambda q(t,\xi,\eta)\right). \tag{66}$$

Integrating (66) with respect to η from 0 to η and using boundary condition (65), we have

$$\begin{aligned}q_\xi(t,\xi,\eta)=&\frac{(R_s^+)^2}{4D_s^+(\check{T}(t))}\lambda+\frac{(R_s^+)^2}{4D_s^+(\check{T}(t))}\\&\times\int_0^\eta\left(q_t(t,\xi,\beta)+\lambda q(t,\xi,\beta)\right)\mathrm{d}\beta.\end{aligned} \tag{67}$$

Integrating (67) with respect to ξ from $-\eta$ to ξ gives the following integro-differential equation (IDE):

$$\begin{aligned}q(t,\xi,\eta)=&\frac{(R_s^+)^2}{4D_s^+(\check{T}(t))}\lambda(\xi+\eta)+\frac{(R_s^+)^2}{4D_s^+(\check{T}(t))}\\&\times\int_{-\eta}^{\xi}\int_0^\eta\left(q_t(t,\alpha,\beta)+\lambda q(t,\alpha,\beta)\right)\mathrm{d}\beta\mathrm{d}\alpha,\end{aligned} \tag{68}$$

where (64) is used.

Second, we apply the method of successive approximation. Let

$$C=\frac{(R_s^+)^2}{4D_s^+(\check{T}(0))e^{E_{D_s^+}/\check{T}(0)}},\quad f(t)=e^{E_{D_s^+}/\check{T}(t)},$$

then from (14), we look for a solution of (68) in the form of

$$q(t,\xi,\eta)=\sum_{n=0}^{\infty}q^n(t,\xi,\eta),$$

where

$$q^0(t,\xi,\eta)=\lambda C(\xi+\eta)f(t), \tag{69}$$

and

$$\begin{aligned}&q^{n+1}(t,\xi,\eta)\\&\quad=Cf(t)\int_{-\eta}^{\xi}\int_0^\eta\left[q_t^n(t,\alpha,\beta)+\lambda q^n(t,\alpha,\beta)\right]\mathrm{d}\beta\mathrm{d}\alpha.\end{aligned} \tag{70}$$

Recall that $\check{T}(t)$ is analytic, and since it is physically impossible for the temperature to reach zero Kelvin, i.e., $\check{T}(t)\neq 0$, then it is reasonable to assume that $\frac{1}{\check{T}(t)}$ is an analytic function in $t\in[0,t_{\max}]$, and thus there exists a constant C_f such that for every nonnegative integer k, the following bound holds:

$$\left|f^{(k)}(t)\right|:=\left|\frac{d^k}{\mathrm{d}t^k}f(t)\right|\le C_f^{k+1}k!. \tag{71}$$

Since the composition of analytic functions is analytic, then $q^0(t,\xi,\eta)$ is an analytic function in $t\in[0,t_{\max}]$ and it can be derived from (69) and (71) that

$$|\partial_t^i q^0(t,\xi,\eta)|\le\lambda CC_f^{i+1}i!(\xi+\eta),\ \forall i\in\mathbb{N},$$

with respect to (ξ,η), uniformly for $t\in[0,t_{\max}]$.

In what follows we are to prove by induction that for any integer $n\ge 0$ the following estimate holds:

$$\begin{aligned}\left|\partial_t^m q^n(t,\xi,\eta)\right|\le&\lambda C^{n+1}C_f^{m+n+1}(C_f+\lambda)^n\\&\times\frac{(m+2n)!}{2^n n!}\frac{\xi^n\eta^n(\xi+\eta)}{n!(n+1)!}.\end{aligned} \tag{72}$$

Assume that (72) holds for an integer $n\ge 0$, then, for any integer $m\ge 0$, we derive from (70) that

$$\begin{aligned}&\left|\partial_t^m q^{n+1}(t,\xi,\eta)\right|\\&=\left|\partial_t^m\left[Cf(t)\int_{-\eta}^{\xi}\int_0^\eta\left[q_t^n(t,\alpha,\beta)+\lambda q^n(t,\alpha,\beta)\right]\mathrm{d}\beta\mathrm{d}\alpha\right]\right|\\&=C\left|\sum_{i=0}^{m}\left[\binom{m}{i}\partial_t^{m-i}f(t)\right.\right.\\&\quad\left.\left.\times\int_{-\eta}^{\xi}\int_0^\eta\left[\partial_t^{i+1}q^n(t,\alpha,\beta)+\lambda\partial_t^i q^n(t,\alpha,\beta)\right]\mathrm{d}\beta\mathrm{d}\alpha\right]\right|.\end{aligned}$$

Through further calculation, we obtain the following estimates

$$\begin{aligned}&\left|\partial_t^m q^{n+1}(t,\xi,\eta)\right|\\&\le C\sum_{i=0}^{m}\left\{\binom{m}{i}C_f^{m+n+2}(m-i)!\right.\\&\quad\times\lambda C^{n+1}\left[C_f+\frac{\lambda}{i+2n+1}\right](C_f+\lambda)^n\\&\quad\left.\times\frac{(i+2n+1)!}{2^n n!}\right\}\frac{\xi^{n+1}\eta^{n+1}(\xi+\eta)}{(n+1)!(n+2)!}\\&\le\lambda C^{n+2}C_f^{m+n+2}(C_f+\lambda)^{n+1}\\&\quad\times\sum_{i=0}^{m}\left[\binom{m}{i}(m-i)!\frac{(i+2n+1)!}{2^n n!}\right]\frac{\xi^{n+1}\eta^{n+1}(\xi+\eta)}{(n+1)!(n+2)!}\\&=\lambda C^{n+2}C_f^{m+n+2}(C_f+\lambda)^{n+1}\\&\quad\times\frac{(m+2(n+1))!}{2^{n+1}(n+1)!}\frac{\xi^{n+1}\eta^{n+1}(\xi+\eta)}{(n+1)!(n+2)!},\end{aligned}$$

where the following equalities have been used:

$$\int_{-\eta}^{\xi}\int_0^\eta\frac{\alpha^n\beta^n(\alpha+\beta)}{n!(n+1)!}\mathrm{d}\beta\mathrm{d}\alpha=\frac{\xi^{n+1}\eta^{n+1}(\xi+\eta)}{(n+1)!(n+2)!},$$

$$\sum_{i=0}^{m}\binom{m}{i}(m-i)!(i+j)!=\frac{(m+j+1)!}{j+1}.$$

By induction, (72) holds for any integer $n\ge 0$.

Finally, the existence of $q(t,\xi,\eta)$ ***and*** $p(t,r,\iota)$ ***can be proved.*** Fixing $m=0$ in (72) gives

$$\left|q^n(t,\xi,\eta)\right|\le\lambda C^{n+1}C_f^{n+1}(C_f+\lambda)^n\frac{(2n)!}{2^n n!}\frac{\xi^n\eta^n(\xi+\eta)}{n!(n+1)!}.$$

Then we can show that the series $\sum_{n=0}^{\infty}q^n(t,\xi,\eta)$ converges absolutely and uniformly. Indeed, the following bound holds:

$$\begin{aligned}|q(t,\xi,\eta)|\le&\sum_{n=0}^{\infty}\left|q^n(t,\xi,\eta)\right|\\\le&\sum_{n=0}^{\infty}\lambda C^{n+1}C_f^{n+1}(C_f+\lambda)^n\frac{(2n)!}{2^n n!}\frac{\xi^n\eta^n(\xi+\eta)}{n!(n+1)!}\\=&\lambda CC_f(\xi+\eta)\sum_{n=0}^{\infty}\phi_1(\xi,\eta;n),\end{aligned}$$

where

$$\phi_1(\xi,\eta;n)=[CC_f(C_f+\lambda)\xi\eta]^n\frac{(2n)!}{2^n n!}\frac{1}{n!\cdot(n+1)!}.$$

Since

$$\begin{aligned}&\lim_{n\to\infty}\frac{\phi_1(\xi,\eta;n+1)}{\phi_1(\xi,\eta;n)}\\&\quad=\lim_{n\to\infty}[CC_f(C_f+\lambda)\xi\eta]\frac{(2n+1)}{(n+1)(n+2)}=0<1,\end{aligned}$$

then from the ratio criterion, the series $\sum_{n=0}^{\infty}\phi_1(\xi,\eta;n)$ is convergent. Consequently, the existence of $q(t,\xi,\eta)$ and $p(t,r,\iota)$ is established, which are analytic in $\mathcal{T}$. Moreover, the following bound holds for $p(t,r,\iota)$

$$|p(t,r,\iota)| \le 2\lambda C C_f r \sum_{n=0}^{\infty}\phi_2(r,\iota;n),$$

where

$$\phi_2(r,\iota;n) = \phi_1(\xi,\eta;n). \quad \square$$

4.2. Invertibility of the transformation (43)

Indeed, the continuity of the kernel $p(t,r,\iota)$ in (43) guarantees the existence of an inverse transformation. We write the inverse transformation as

$$\tilde{w}(t,r) = \tilde{c}(t,r) + \int_r^1 \rho(t,r,\iota)\tilde{c}(t,\iota)\mathrm{d}\iota, \tag{73}$$

then we could derive from (43) and (73) that the kernel $\rho(t,r,\iota)$ needs to satisfy

$$\rho(t,r,\iota) = p(t,r,\iota) + \int_r^{\iota} p(t,r,\sigma)\rho(t,\sigma,\iota)\mathrm{d}\sigma. \tag{74}$$

In order to solve Eq. (74), a similar (successive approximation) procedure as in Section 4.1 can be followed, see also, Krstic and Smyshlyaev (2008, Section 4.4). A similar well-posedness result for its inverse can also be obtained and this derivation is omitted here.

Note also that the initial condition $\tilde{w}_0(r)$ for the target $\tilde{w}$-system (44)–(47) is determined by $\hat{c}_0(r)$ and $\rho_0(r,\iota) = \rho(0,r,\iota)$. Indeed, from (42) and (73), $\tilde{w}_0(r)$ can be calculated as

$$\tilde{w}_0(r) = c_0(r) - \hat{c}_0(r) + \int_r^1 \rho_0(r,\iota)[c_0(\iota) - \hat{c}_0(\iota)]\mathrm{d}\iota.$$

4.3. Exponential convergence of the observer

Some assumptions and simplifications have been made to ease the analysis. For completeness and clarity we summarize these assumptions and simplifications before stating our main result.

(A1) To derive an output inversion function, i.e., to recover $c_{ss}^{+}(t)$ from the voltage measurement, we have assumed that $T(t)$ is a time-varying function independent of concentrations. We have used the notation $\check{T}(t)$ and compute its value from Eq. (23). For this assumption to hold, some underlying simplifications and assumptions have been made:
  (i) Parameters $R_f^{\pm}(T(t))$ and $r_{\mathrm{eff}}^{\pm}(T(t))$ are approximated by $\check{R}_f^{\pm}(t) \triangleq R_f^{\pm}(T_{\mathrm{amb}}(t))$ and $\check{r}_{\mathrm{eff}}^{\pm}(t) \triangleq r_{\mathrm{eff}}^{\pm}(T_{\mathrm{amb}}(t))$.
  (ii) Functions $U^{\pm}(\cdot,T(t))$ are assumed to be independent of concentrations, and their dependence on $T(t)$ has been replaced with dependence on $T_{\mathrm{amb}}(t)$. We have used the notation $\check{U}_1^{\pm}(t) \triangleq U^{\pm}(c_{ss}^{\pm}(t),T_{\mathrm{amb}}(t))$ and $\check{U}_2^{\pm}(t) \triangleq U^{\pm}(\bar{c}_s^{\pm}(t),T_{\mathrm{amb}}(t))$.

(A2) To derive an output inversion function, diffusion of lithium in the negative electrode has been simplified. This is done by assuming a polynomial solution profile for the diffusion dynamics in the negative electrode.

(A3) For observer design, we have used $\check{T}(t)$ to replace $T(t)$.

(A4) For observer design, functions $I(t)$, $U^{\pm}(\cdot,T(t))$, $V(t)$ and $\partial U^{\pm}/\partial T(\cdot,T(t))$ are assumed to be piecewise analytic.

Now, our main result can be presented. Consider an appropriate time interval $[0,t_{\max}]$ for the assumed regularities in (A4) to hold. With the well-posedness of the kernel function in the transformation (43) together with the invertibility of the transformation, the following main theorem holds.

Theorem 4. *Let $t \in [0,t_{\max}]$. Under the simplifications and assumptions* (A1)–(A4)*, if*

$$\lambda < \frac{1}{4(R_s^{+})^2}\min_{t\ge 0}\{D_s^{+}(\check{T}(t))\},$$

then for any initial value $\hat{c}(0,\cdot) \in L^2(0,1)$, the observer error $\tilde{c}$-system (39)–(42) is exponentially stable at $\tilde{c} \equiv 0$ in the L^2 norm, which means the designed observer (35)–(38) is exponentially convergent to the system (31)–(34).

Proof. It follows directly from (51) that

$$\|\tilde{w}(t,\cdot)\| \le \|\tilde{w}(0,\cdot)\| e^{-\left(\frac{D_s^{+}(\check{T}(t))}{4(R_s^{+})^2}-\lambda\right)t}. \tag{75}$$

From the state transformations (43) and (73), the equivalence of the states $\tilde{c}(t,r)$ and $\tilde{w}(t,r)$ is established, i.e., there exist positive constants M_1, M_2 such that

$$M_1\|\tilde{w}(t,\cdot)\| \le \|\tilde{c}(t,\cdot)\| \le M_2\|\tilde{w}(t,\cdot)\|. \tag{76}$$

Then, the proof is completed with (75) and (76). $\square$

Remark 5. Theorem 4 is rigidly proved under the assumption that the averaged internal temperature is independent of the lithium ion concentrations in the electrodes; computed from the linear ODE (23). Here, we would like to clarify that these assumptions are posed solely for the theoretical derivations. Indeed, in the next section we are to present some simulation results showing that the original unsimplified equation for the averaged internal temperature (17) can be used in the implementation of the estimation algorithm, which depends on lithium ion concentrations in the electrodes, and still achieve convergence of the SoC estimate. Since only estimates of lithium ion concentration are available to compute the internal averaged temperature, we are actually computing an open-loop estimate calculated from (17) and use the notation $\hat{T}(t)$, i.e.,

$$\begin{aligned}
&\rho^{\mathrm{avg}}c_P\frac{\mathrm{d}\hat{T}(t)}{\mathrm{d}t}(t)\\
&\quad= h_{\mathrm{cell}}\left(T_{\mathrm{amb}}(t)-\hat{T}(t)\right)\\
&\qquad+ I(t)\frac{R\hat{T}(t)}{\alpha F}\left[\sinh^{-1}\left(\frac{1}{2\hat{i}_0^{+}(t)}\frac{I(t)}{a^{+}L^{+}}\right)\right.\\
&\qquad\left.+\sinh^{-1}\left(\frac{1}{2\hat{i}_0^{-}(t)}\frac{I(t)}{a^{-}L^{-}}\right)\right]\\
&\qquad+\left(\frac{R_{\mathrm{f}}^{+}(\hat{T}(t))}{a^{+}L^{+}}+\frac{R_{\mathrm{f}}^{-}(\hat{T}(t))}{a^{-}L^{-}}-R_c\right)I(t)^2\\
&\qquad- I(t)\left[U^{+}(\hat{c}_{ss}^{+}(t),\hat{T}(t))-U^{-}(\hat{c}_{ss}^{-}(t),\hat{T}(t))\right]\\
&\qquad+ I(t)\left\{U^{+}(\hat{\bar{c}}_s^{+}(t),\hat{T}(t))-U^{-}(\hat{\bar{c}}_s^{-}(t),\hat{T}(t))\right.\\
&\qquad\left.-\hat{T}(t)\left[\frac{\partial U^{+}(\hat{\bar{c}}_s^{+}(t),\hat{T}(t))}{\partial T}-\frac{\partial U^{-}}{\partial T}(\hat{\bar{c}}_s^{-}(t),\hat{T}(t))\right]\right\},
\end{aligned} \tag{77}$$

where $\hat{i}_0^{\pm}(t)$ are computed from (12) with concentration values replaced by their estimates.

In the original state variables and unnormalized coordinates, the observer for lithium-ion concentration in the positive electrode reads

$$\frac{\partial \hat{c}_s^+}{\partial t}(t, r_s) = \frac{D_s^+(\hat{T}(t))}{r_s^2}\frac{\partial}{\partial r_s}\left[r_s^2 \frac{\partial \hat{c}_s^+}{\partial r_s}(t, r_s)\right] + \bar{p}_1(t, r_s)(c_{ss}^+(t) - \hat{c}_{ss}^+(t)), \tag{78}$$

$$\frac{\partial \hat{c}_s^+}{\partial t}(t, 0) = 0, \tag{79}$$

$$\frac{\partial \hat{c}_s^+}{\partial r}(t, R_s) = \frac{I(t)}{D_s^+(\hat{T}(t))a^+FL^+} + \bar{p}_{10}(t)(c_{ss}^+(t) - \hat{c}_{ss}^+(t)), \tag{80}$$

with

$$\bar{p}_1(t, r_s) = \frac{p_1(t, \frac{r_s}{R_s})}{r_s}, \quad \bar{p}_{10}(t) = \frac{p_{10}(t)}{R_s}. \tag{81}$$

The SoC estimation can then be derived from (19) and (21), with $c_s^+(t, r_s)$ replaced by their estimated values $\hat{c}_s^+(t, r_s)$. Additionally, estimates $\hat{c}_s^-(t, r_s)$ and $\hat{c}_{ss}^-(t, r_s)$ on the negative electrode can be computed from (28)–(29), with the estimates $\hat{c}_{ss}^+(t, r_s)$ and $\hat{c}_{ss}^+(t, r_s)$ on the positive electrode obtained from (78)–(81) and the open-loop estimate $\hat{T}(t)$ from (77).

5. Simulation results

The ambient temperature is assumed to be constant; $T_{amb} = 298$ [K] $= 24.85$ [°C]. Simulations are performed with parameters of a $LiCoO_2$–LiC_6 cell. Parameters and OCP functions $U^{\pm}$ are borrowed from Mao, Tiedemann, and Newman (2014) and the references within. Note that the OCP functions depend on the internal average temperature and here a linear approximation is employed:

$$U^{\pm}(c_{ss}^{\pm}(t), T) = U^{\pm}(c_{ss}^{\pm}(t), T_{amb}) + \frac{\partial U^{\pm}(c_{ss}^{\pm}(t), T_{amb})}{\partial T}(T - T_{amb}).$$

The magnitude of input current is described in terms of the cell C-rate (per unit area), which is computed from

$$\text{C-rate} = F\frac{\min\left\{\varepsilon_s^+ L^+ c_s^{+,\max}, \varepsilon_s^- L^- c_s^{-,\max}\right\}}{3600[\text{s}]}.$$

5.1. Simulation tests

Simulation tests are performed to evaluate the effectiveness of the proposed observer with two different current profiles: a square profile (constant charge, discharge and rest) and a current profile obtained from the Urban Dynamometer Driving Schedule (UDDS). For each current profile two cases of measurements are considered: voltage measurements generated from the SPM-T model and voltage measurements generated from the DFN model serving as true data. To generate voltage measurements, lithium concentration in the negative electrode is initialized at 80% of the maximum value and lithium concentration in the positive electrode is initialized at 50% of the maximum value. For the observer, lithium concentration in the negative electrode is initialized at 50% of the maximum value and the one in the positive electrode is initialized at 67% of the maximum value. The tuning parameter λ in the observer is set as -1 for all tests.[3]

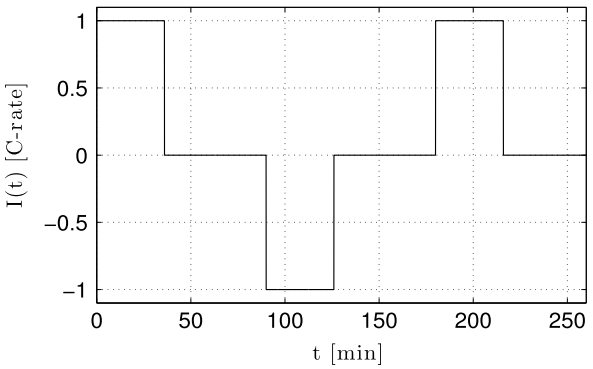

Fig. 2. Current profile.

5.1.1. Simulation with square current profile

Figs. 2–5 correspond to the first set of simulation tests, which use a square current profile shown in Fig. 2. The current consists of repeated cycles of: 36 min of 1 C-rate constant discharging followed by 54 min of resting, i.e., zero input, then 36 min of 1 C-rate constant charging ending with 54 min of zero input. Only the first 250 min of the simulation results are shown in the figures. True and estimated SoC are shown in Fig. 3 using (a) SPM-T measurements and (b) DFN measurements. The initial errors in SoC estimation are due to intentionally chosen, incorrect initialization of lithium concentrations. Convergence of output voltage coincides with convergence of SoC, and this is shown in Fig. 4. The estimate of internal average temperature is shown in Fig. 5 using voltage measurements from the (a) SPM-T model and (b) DFN model; compared against the true average temperature of the respective models. Note that, since the internal average temperature is monitored in an open-loop fashion, one needs to correctly initialize its value. This condition is satisfied at thermal equilibrium, i.e., the internal average temperature of the battery coincides with the ambient temperature.

5.1.2. Simulation with UDDS current profile

Figs. 6–9 correspond to simulation tests using a current input derived from a set of UDDS data and scaled to a current density profile within the range of ±4 C-rate of the battery. This current profile, shown in Fig. 6, is representative of current demands in automotive applications. SoC estimation is shown in Fig. 7 with the initial errors coming from incorrect initialization. As seen in Fig. 8, convergence of the output voltage coincides with convergence of the SoC as well. Finally, Fig. 9 compares the open-loop estimates of internal average temperature with the true internal average temperature from the (a) SPM-T model and (b) DFN model.

Fig. 10 shows (a) the difference in output voltage values between SPM-T model and SPM and (b) the difference in temperature values from SPM-T model and DFN model for constant discharge currents. One can see that the difference in output voltage values from SPM-T model and SPM accentuates at high currents rate (a) while temperature values from SPM-T model and DFN model remain relatively close for currents as high as 4 C-rate (b).

5.2. Numerical implementations

Numerical implementations of the SPM-T and the DFN models follow the equations presented in Sections 2.1 and 2.2, respectively. A finite volume method is used for the spatial discretization

[3] Ideally, the convergence rate of the designed observer can be made arbitrarily high by choosing a small enough λ, i.e., a large enough $|\lambda|$. However, since accurate/direct measurement of boundary concentration is not available and approximations required in output inversion unavoidably introduce error in the (calculated) boundary measurement, there exists a design trade-off between high convergence rate of the observer and effective attenuation of the approximation error/measurement noise. In particular, choosing large values for $|\lambda|$ makes the system more sensitive to measurement noise and results in larger estimation errors.

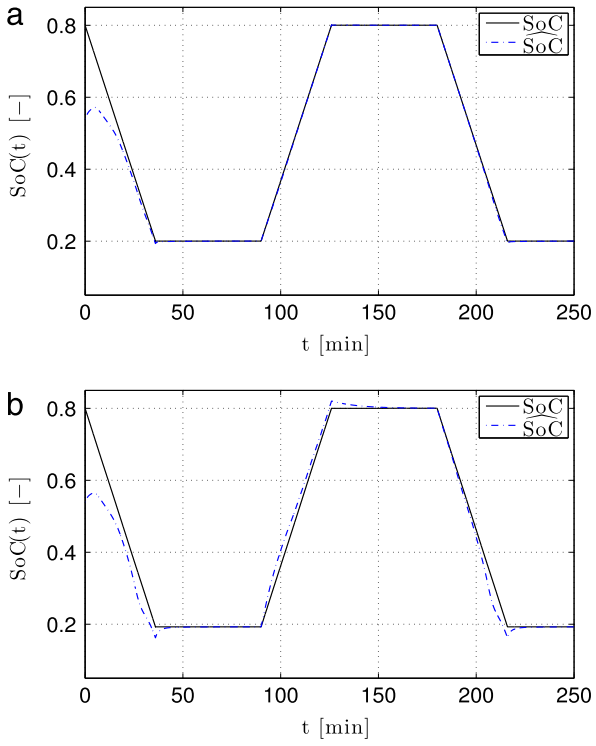

Fig. 3. True and estimated SoC. (a). Observer with SPM-T measurements. (b). Observer with DFN measurements.

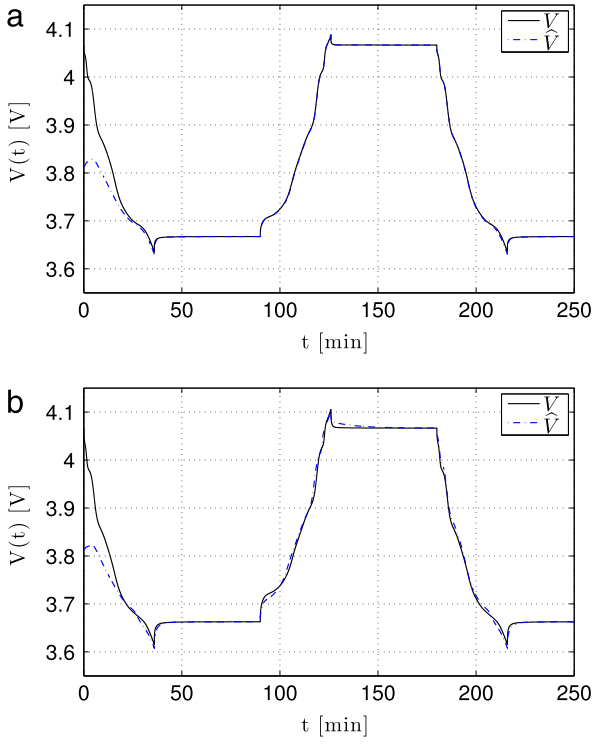

Fig. 4. True and estimated voltage. (a). Observer with SPM-T measurements. (b). Observer with DFN measurements.

of PDEs in the models, and then the Euler-backward method is used for the temporal discretization of the resulting system of ODEs. The observer is implemented using the same discretization procedure. Note that in the numerical implementation of the observer, lithium

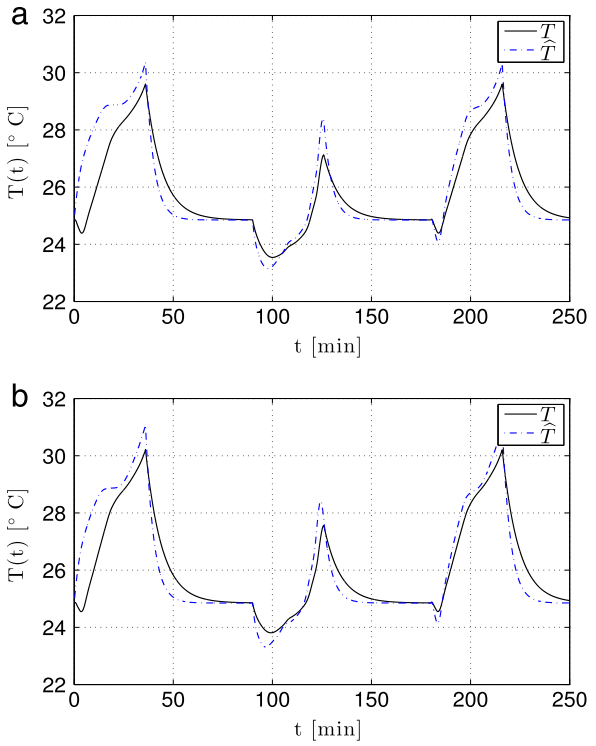

Fig. 5. True and estimated internal average temperature. (a). Observer with SPM-T measurements. (b). Observer with DFN measurements.

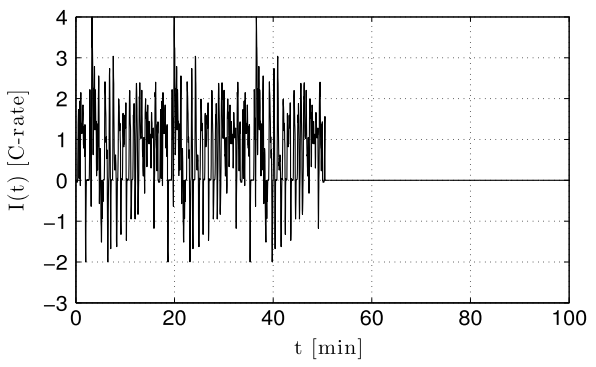

Fig. 6. Current profile.

concentration in the negative electrode is approximated by the polynomial profile presented in Subramanian et al. (2005), as described briefly in Section 3.2.

For the numerical implementation of the kernel function $p(t, r, \iota)$ and the computation of the observer gain, a trapezoidal approximation of the IDE (68) is used to obtain an ODE, which is then discretized in time with the Euler-backward method. As mentioned in Section 4, time normalization $t' = D_s^+(T(t))/(R_s^+)^2 t$ by the temperature-dependent function is not preferable; here the normalization is performed by a constant instead, i.e., $t' = D_s^+(T_{\text{amb}})/(R_s^+)^2 t$.

6. Conclusions and future work

This paper discusses the problem of SoC estimation for the lithium-ion batteries based on a thermal–electrochemical model. In this regard, an infinite-dimensional Luenberger observer is proposed. For the transformation between the observer error system

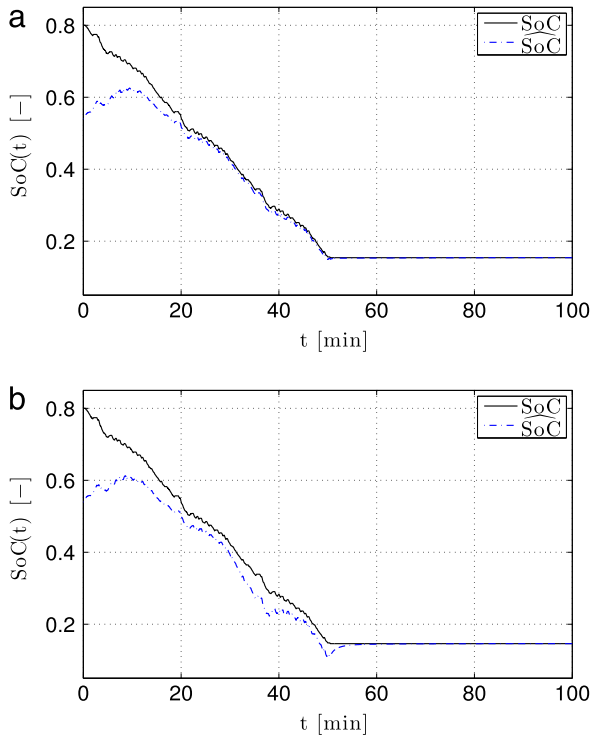

Fig. 7. True and estimated SoC. (a). Observer with SPM-T measurements. (b). Observer with DFN measurements.

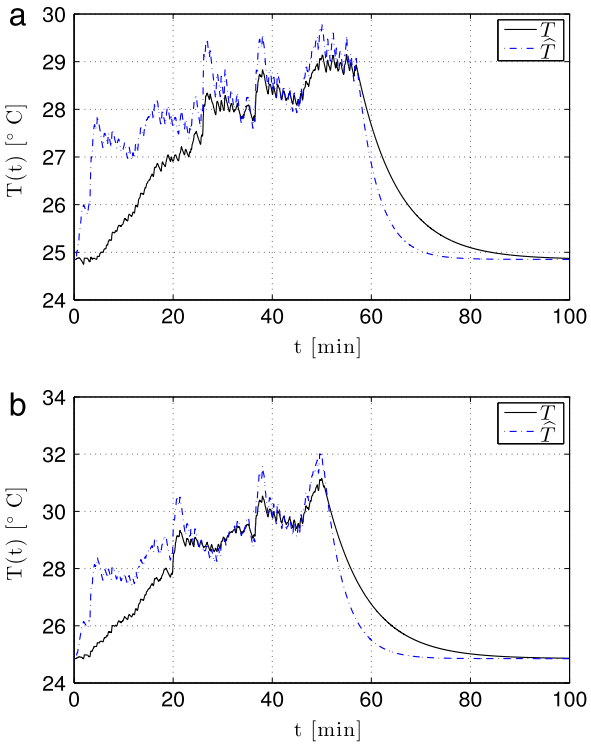

Fig. 9. True and estimated interval average temperature. (a). Observer with SPM-T measurements. (b). Observer with DFN measurements.

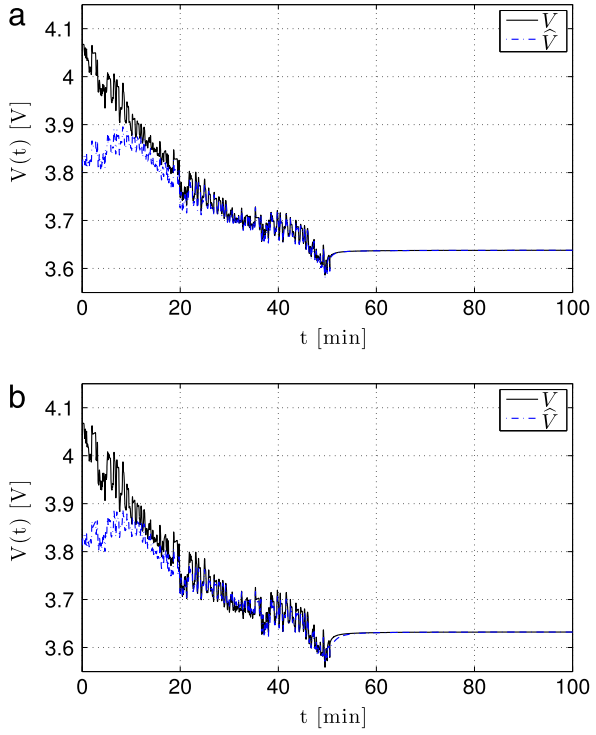

Fig. 8. True and estimated voltage. (a). Observer with SPM-T measurements. (b). Observer with DFN measurements.

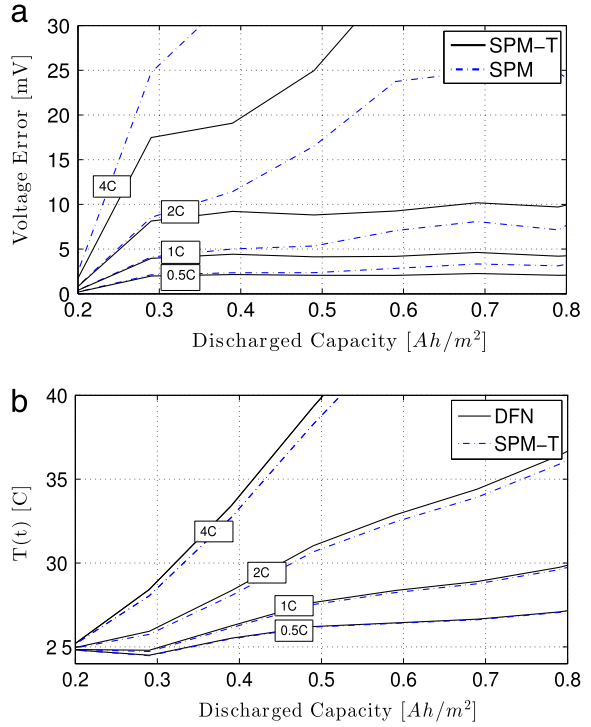

Fig. 10. SPM-T model validation. (a) Output voltage error between SPM and DFN, and between SPM-T and DFN. (b) Internal averaged temperature computed from the DFN model and from the SPM-T model.

and the exponentially stable target system, well-posedness of the time-varying PDE backstepping kernel functions are rigorously proved. Then, exponential stability of the observer error system is established, which proves effectiveness of the designed observer.

We consider this result as an additional step in the effort to design estimation (and control) algorithms for lithium-ion batteries from electrochemical models, without relying on the discretization of the PDEs in these models.

The observer requires only one design/tuning parameter as compared with the possibly large number of tuning parameters required in estimation methods based on finite dimensional battery models, e.g., EKF. Compared with estimation based on the infinite dimensional SPM alone, it takes into account the temperature dependence of model parameters and catches the battery responses better than SPM, especially at high C-rates. Simultaneously, the internal average temperature can be monitored in an open-loop fashion.

Some simplifications are made in this paper, and their relaxation could be considered as a future research direction. Another possible extension is to retain the concentration dynamics in the negative electrode and design one observer for each electrode (Moura, Bribiesca Argomedo, Federico, Klein, Mirtabatabaei, & Krstic, 2016). One could also consider multiple active materials in the electrodes (Camacho-Solorio, Klein, Mirtabatabaei, Krstic, & Moura, 2016) or add models for degradations (e.g., capacity fade) to the battery model (Ramadesigan, Boovaragavan, Arabandi, Chen, Tsukamoto, Braatz, & Subramanian, 2009). Observer design for the battery internal, core and surface (Lin, Perez, Mohan, Siegel, Stefanopoulou, Ding, & Castanier, 2014), or even the distributed (Kim, Mohan, Siegel, Stefanopoulou, & Ding, 2013) temperature is a subject worth investigating as well.

Acknowledgment

The authors would like to acknowledge Jean-Michel Coron for suggesting the application of the abstract evolution equation theory in the well-posedness derivation of the solution to the PDE systems with time-varying coefficients.

References

Camacho-Solorio, L., Klein, R., Mirtabatabaei, A., Krstic, M., & Moura, S. (2016). State estimation for an electrochemical model of multiple-material lithium-ion batteries. *ASME Dynamic Systems and Control Conference*.

Chaturvedi, N., Klein, R., Christensen, J., Ahmed, J., & Kojic, A. (2010). Algorithms for advanced battery-management systems. *IEEE Control Systems Magazine*, *30*(3), 49–68.

Chiasson, J., & Vairamohan, B. (2005). Estimating the state of charge of a battery. *IEEE Transactions on Control Systems Technology*, *13*(3), 465–470.

Chu, S., & Majumdar, A. (2012). Opportunities and challenges for a sustainable energy future. *Nature*, *488*(7411), 294–303.

Doyle, M., Fuller, T. F., & Newman, J. (1993). Modeling of galvanostatic charge and discharge of the lithium/polymer/insertion cell. *Journal of the Electrochemical Society*, *140*(6), 1526–1533.

Guo, M., Sikha, G., & White, R. E. (2011). Single-particle model for a lithium-ion cell: thermal behavior. *Journal of the Electrochemical Society*, *158*(2), A122–A132.

Haran, B. S., Popov, B. N., & White, R. E. (1998). Determination of the hydrogen diffusion coefficient in metal hydrides by impedance spectroscopy. *Journal of Power Sources*, *75*(1), 56–63.

Izadi, M., & Dubljevic, S. (2015). Backstepping output-feedback control of moving boundary parabolic pDEs. *European Journal of Control*, *21*, 27–35.

Kim, Youngki, Mohan, Shankar, Siegel, Jason B., Stefanopoulou, Anna G., & Ding, Yi. (2013). The estimation of radial temperature distribution in cylindrical battery cells under unknown cooling conditions. In *52nd IEEE conference on decision and control* (pp. 5680–5685).

Klein, R., Chaturvedi, N., Christensen, J., Ahmed, J., Findeisen, R., & Kojic, A. (2013). Electrochemical model based observer design for a lithium-ion battery. *IEEE Transactions on Control Systems Technology*, *21*(2), 289–301.

Krstic, M., & Smyshlyaev, A. (2008). *Boundary control of PDEs: A course on backstepping designs*. SIAM.

Lin, Xinfan, Perez, Hector E., Mohan, Shankar, Siegel, Jason B., Stefanopoulou, Anna G., Ding, Yi, & Castanier, Matthew P. (2014). A lumped-parameter electro-thermal model for cylindrical batteries. *Journal of Power Sources*, *257*, 1–11.

Mao, J., Tiedemann, W., & Newman, J. (2014). Simulation of li-ion cells by dualfoil model under constant-resistance load. *ECS Transactions*, *58*(48), 71–81.

Moura, S., Chaturvedi, N., & Krstic, M. (2014). Adaptive partial differential equation observer for battery state-of-charge/state-of-health estimation via an electrochemical model. *Journal of Dynamic Systems, Measurement, and Control*, *136*(1), 011015.

Moura, S. J., Bribiesca Argomedo, F., Federico, Klein, R., Mirtabatabaei, A., & Krstic, M. (2016). Battery state estimation for a single particle model with electrolyte dynamics. *IEEE Transactions on Control System Technology*, *25*, 1086–1090.

Pazy, A. (1983). *Semigroups of linear operators and applications to partial differential equations*. New York: Springer-Verlag.

Plett, Gregory L. (2004). Extended Kalman filtering for battery management systems of LiPB-based HEV battery packs: Part 2. Modeling and identification. *Journal of Power Sources*, *134*(2), 262–276.

Ramadesigan, Venkatasailanathan, Boovaragavan, Vijayasekaran, Arabandi, Mounika, Chen, Kejia, Tsukamoto, Hisashi, Braatz, Richard, & Subramanian, Venkat (2009). Parameter estimation and capacity fade analysis of lithium-ion batteries using first-principles-based efficient reformulated models. *ECS Transactions*, *19*(16), 11–19.

Ramadesigan, Venkatasailanathan, Northrop, Paul W. C., De, Sumitava Santhanagopalan, Shriram, Braatz, Richard D., & Subramanian, Venkat R. (2012). Modeling and simulation of lithium-ion batteries from a systems engineering perspective. *Journal of the Electrochemical Society*, *159*(3), R31–R45.

Santhanagopalan, S., & White, R. E. (2006). Online estimation of the state of charge of a lithium ion cell. *Journal of Power Sources*, *161*(2), 1346–1355.

Smyshlyaev, A., & Krstic, M. (2003). Explicit state and output feedback boundary controllers for partial differential equations. *Journal of Automatic Control*, *13*(2), 1–9.

Smyshlyaev, A., & Krstic, M. (2005). On control design for PDEs with space-dependent diffusivity or time-dependent reactivity. *Automatica*, *41*(9), 1601–1608.

Stewart, S., Christensen, J., Chaturvedi, N., & Kojic, A. (2015). Challenges in batteries for electric vehicles. In *Frontiers of engineering: Reports on leading-edge engineering from the 2014 symposium*.

Subramanian, V. R., Diwakar, V. D., & Tapriyal, D. (2005). Efficient macro-micro scale coupled modeling of batteries. *Journal of the Electrochemical Society*, *152*(10), A2002–A2008.

Tang, S.-X., Wang, Y., Sahinoglu, Z., Wada, T., Hara, S., & Krstic, M. (2015). State-of-charge estimation for lithium-ion batteries via a coupled thermal–electrochemical model. *American Control Conference*, 5871–5877.

Tang, S.-X., & Xie, C. (2011a). Stabilization for a coupled PDE–ODE control system. *Journal of the Franklin Institute*, *348*(8), 2142–2155.

Tang, S.-X., & Xie, C. (2011b). State and output feedback boundary control for a coupled pDE-ODE system. *Systems & Control Letters*, *60*, 540–545.

Tanim, Tanvir R., Rahn, Christopher D., & Wang, Chao-Yang (2015). State of charge estimation of a lithium ion cell based on a temperature dependent and electrolyte enhanced single particle model. *Energy*, *80*, 731–739.

Thomas, K., Newman, J., & Darling, R. (2002). Mathematical modeling of lithium batteries. In *Advances in lithium-ion batteries* (pp. 345–392). New York, NY USA: Kluwer Academic/Plenum Publishers, (Ch. 12).

Shu-Xia Tang received her Ph.D. in Mechanical Engineering in 2016 from the Department of Mechanical & Aerospace Engineering, University of California, San Diego, USA. She is currently a postdoctoral research fellow and lecturer at the Department of Applied Mathematics, University of Waterloo, Canada. Her main research interests are control and estimation in distributed parameter systems. Recent research also includes optimal actuator and sensor design problems.

Leobardo Camacho-Solorio received the B.S. degree in Mechatronics Engineering from Tecnologico de Monterrey, Queretaro in 2014. He is now working towards the Ph.D. degree in Mechanical Engineering at the University of California, San Diego. His research interests include estimation and control of systems described by partial differential equations with applications to electrochemical models of lithium-ion batteries.

Yebin Wang received the B.Eng. degree in Mechatronics Engineering from Zhejiang University, Hangzhou, China, in 1997, M.Eng. degree in Control Theory & Control Engineering from Tsinghua University, Beijing, China, in 2001, and Ph.D. in Electrical Engineering from the University of Alberta, Edmonton, Canada, in 2008. Dr. Wang has been with Mitsubishi Electric Research Laboratories in Cambridge, MA, USA, since 2009, and now is a Senior Principal Research Scientist. From 2001 to 2003 he was a Software Engineer, Project Manager, and Manager of R&D Dept. in industries, Beijing, China. His research interests include nonlinear control and estimation, optimal control, adaptive systems and their applications including mechatronic systems.

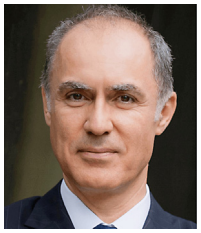

Miroslav Krstic is Distinguished Professor of Mechanical and Aerospace Engineering, holds the Alspach endowed chair, and is the founding director of the Cymer Center for Control Systems and Dynamics at UC San Diego. He also serves as Associate Vice Chancellor for Research at UCSD. As a graduate student, Krstic won the UC Santa Barbara best dissertation award and student best paper awards at CDC and ACC. Krstic is Fellow of IEEE, IFAC, ASME, SIAM, and IET (UK), Associate Fellow of AIAA, and foreign member of the Academy of Engineering of Serbia. He has received ASME Oldenburger Medal, ASME Nyquist Lecture Prize, ASME Paynter Outstanding Investigator Award, the PECASE, NSF Career, and ONR Young Investigator awards, the Axelby and Schuck paper prizes, the Chestnut textbook prize, and the rst UCSD Research Award given to an engineer. Krstic has also been awarded the Springer Visiting Professorship at UC Berkeley, the Distinguished Visiting Fellowship of the Royal Academy of Engineering, the Invitation Fellowship of the Japan Society for the Promotion of Science, and honorary professorships from four universities in China. He serves as Senior Editor in IEEE Transactions on Automatic Control and Automatica, as editor of two Springer book series, and has served as Vice President for Technical Activities of the IEEE Control Systems Society and as chair of the IEEE CSS Fellow Committee. Krstic has coauthored twelve books on adaptive, nonlinear, and stochastic control, extremum seeking, control of PDE systems including turbulent ows, and control of delay systems.